Nanostructured Hydrotropes Caged Cytochrome c with Boosted Stability in Harsh Environments: A Molecular Insights

Pranav Bharadwaj[†, ϕ], Dheeraj Kumar Sarkar[§, ψ, ϕ], Meena Bisht[‡], Sachin M. Shet[†], S. K. Nataraj,[†] Veeresh Lokesh[‡], Gregory Franklin*[,‡], Jan Brezovsky*[,§, ψ], and Dibyendu Mondal*[,†,‡]

† Centre for Nano and Material Sciences, Jain University, Bangalore 562112, India

§ Laboratory of Biomolecular Interactions and Transport, Department of Gene Expression, Institute of Molecular Biology and Biotechnology, Faculty of Biology, Adam Mickiewicz University, Uniwersytetu Poznanskiego 6, 61-614 Poznan, Poland

ψ International Institute of Molecular and Cell Biology in Warsaw, Ks Trojdena 4, 02-109 Warsaw, Poland

‡ Institute of Plant Genetics (IPG), Polish Academy of Sciences, Strzeszyńska 34, 60-479 Poznań, Poland

*Corresponding authors

ϕ These authors have contributed equally to this work.

ABSTRACT: Green and nanostructured catalytic media are vital in biocatalysis to attenuate the denaturation tendency of biocatalysts under severe reaction conditions. Hydrotropes with multifaceted physiochemical properties can be envisaged as promising systems for sustainable protein packaging. Herein, the suitability of adenosine-5'-triphosphate (ATP) and cholinium salicylate ([Cho][Sal]) ionic liquid (IL) to form nanostructures and to nanoconfine Cytochrome c (Cyt c) were disclosed envisioning enhancement of stability and activity under multiple stresses. Experimental and computational validations were undertaken to explain nanostructuring phenomenon of ATP and IL, structural organizations of nanoconfined Cyt c, and site-specific interactions that stabilize protein structure. Both, ATP and IL form nanostructures in aqueous media and caged Cyt c via multiple non-specific soft interactions. Remarkably, the engineered molecular nano-cages of ATP (5-10 mM), IL (300 mg/mL), and ATP+IL around Cyt c resulted in 9-72 folds higher peroxidase activity than native Cyt c with exceptionally high thermal tolerance (110 °C). The polar interactions mediated by hydrotropes with the cardiolipin binding site of Cyt c well corroborated with the increased peroxidase activity. Further, higher activity trends were observed in the presence of urea, GuHCl, and trypsin without any protein degradation. Specific binding of hydrotropes at highly mobile regions of Cyt c (Ω 40-54 residues) and enhanced H-bonding with Lys and Arg offered excellent stability under extreme conditions. Additionally, ATP effectively counteracted reactive oxygen species (ROS) induced denaturation of Cyt c, which was enhanced by [Sal] counterpart of IL. Overall, this study explored the robustness of nanostructured hydrotropes having a higher potential for protein packaging with improved stability and activity in extreme conditions. Thus, the present work brings out a novel strategy for real-time industrial biocatalysis to protect mitochondrial cells from ROS-instigated apoptosis.

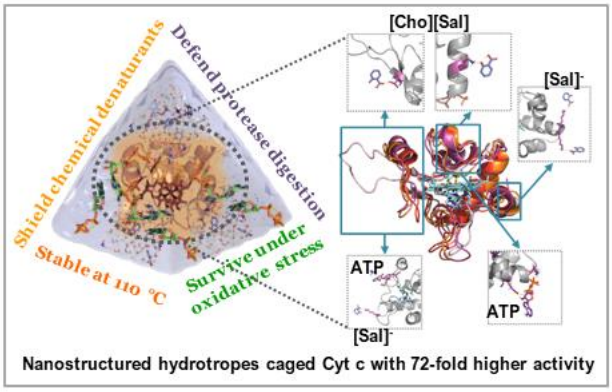

INTRODUCTION

Adenosine-5'-triphosphate (ATP) has shown multifaceted functions which include its participation in the electron transport chain, acting as the energy currency of cells, holding the key for caspase-9-activated apoptosis, and taking part in transcription by revamping chromatin complexes.[1-3] The role of physiological concentration of ATP in preventing thermally induced protein aggregation in mammalian cells was demonstrated by *Nguyen and Benusaude*,[4] and the answer regarding the regulation of high concentration of ATP (2-10 mM) in the cell is unveiled by *Patel and co-workers,* wherein ATP is claimed as a biological hydrotrope.[5] The term 'hydrotrope' was coined by *Neuberg* for the amphiphilic molecules having a characteristic range of minimum hydrotrope concentration which augment the solubility of partially soluble organic or hydrophobic substances in water.[6-7] This opened a new channel to explore ATP in the medicinal field to treat Parkinson's and Alzheimer-like diseases by preventing phase separation of biological fluids which causes amyloid fibrillations.[8-9] Solubilizing tendency of ATP was attributed to its non-specific aggregation, charge reinforcement, and self-

assembly through hydrophobic interactions (Figure 1a).[10-11] Thus, the hydrotropic mechanism of ATP follows both Neuberg and Hofmeister effects.[12] Self-aggregated ATP is found to provide thermal stability to lysozyme, malate dehydrogenase, and ubiquitin,[13] it is important to understand how the self-aggregation property of ATP is useful in protein packaging under multiple stresses, which has not been studied so far.

Unlike ATP, various amphiphilic nanostructured solvents have recently emerged with promising applications in energy-efficient bioprocesses.[14] Due to their highly manipulative nature, ionic liquids (ILs) gained potential interest in increasing enzyme solubility and thermal stability.[15] Interestingly, few bio-based ILs of cholinium family have shown hydrotropic property[16] with greater hydrophobicity and enhanced the nanostructuring of amphiphilic solute in aqueous media.[17] Earlier reports showed cholinium-based ILs for protein packaging with long-term stability and activity,[15] but there is a paucity of understanding of the underlying mechanisms by which hydrotropic ILs (potential amphiphilic molecules) can regulate the protein stability and activity.[18] In this regard, the IL with salicylate counterpart dragged our attention as it contains carboxylic, hydroxyl groups along with a hydrophobic aromatic ring which features the salicylate ion to show multi-interaction sites in the aqueous medium (Figure 1b).[19-20] Additionally, salicylic acid is an important phytohormone that alters the mitochondrial processes by amplifying reactive oxygen species concentration and impels cells to undergo programmed cell death.[21-22] In the apoptosis process, ATP also plays a crucial role in caspase-9 activation stimulated by cytochrome c (Cyt c) release from mitochondria.[23] Since both ATP and salicylate are in a way coupled to Cyt c, the latter was chosen as a model protein in this study (Figure 1c), and ATP and choline salicylate ([Cho][Sal]) IL as the nanostructured hydrotropes.

Cyt c is a mitochondrial-based 13 kDa monomeric protein comprising about 104 residues and is widely distributed across eukaryotes, bacteria, and archaea.[24] Despite its significant role in electron transfer, this protein is of great interest in many technological applications like biosensors, synthetic receptors, molecular imprinting and more.[24] Cyt c also shows peroxidase-like activity and serves as a biocatalyst in several catalytic transformations.[24] The protein is highly vulnerable to denaturation under prevailing stress conditions like extreme temperatures, oxidative stress, and proteolytic and chemical denaturants.[25] Recently, a surface modification strategy by using quantum dots, metal-organic frameworks,[26] and DNA was reported to enhance the stability of Cyt C.[25,27] However, the stability of the protein confined in hydrotropes systems is not yet reported. Considering the hydrotropism and probability of nanostructuring,[24] the present study aims to cage Cyt c in ATP and [Cho][Sal] IL-based hydrotropes and thereby improving activity and stability of the protein in habitual and harsh environments (such as high temperature, chemical denaturants, protease digestion, and oxidative stress). In this direction, detailed experimental and *in silico* approaches were undertaken to study the molecular level structure-function relationship of nanoconfined Cyt c in ATP, [Cho][Sal] and ATP + IL to develop a novel and sustainable solvent manipulation strategy for dynamic protein packaging and robust biocatalysis.

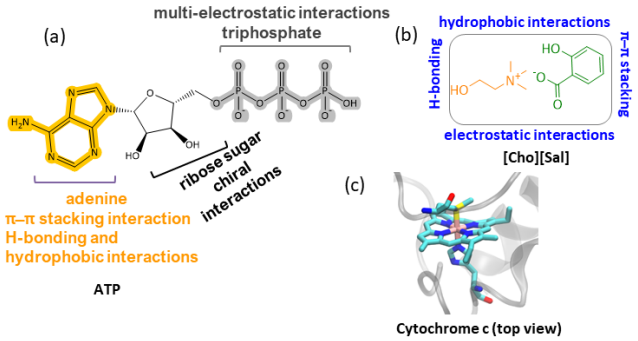

Figure 1: Chemical structures and structural features of (a) ATP and (b) [Cho][Sal] ionic liquid with possible interaction sites available. (c) The model active site structure of Cyt c is based on the crystallographic structure of bovine heart Cyt c (PDB code: 2B4Z) at 1.5 Å resolution.

RESULTS AND DISCUSSION

ATP and [Cho][Sal] IL as nanostructured hydrotropes

To understand to what extent the IL affects the self-aggregation of ATP which is vital for its role as a biological hydrotrope, we performed molecular dynamics (MD) simulations of 5 mM ATP, 300 mg/mL [Cho][Sal], and their mixture. The pair-wise interactions of ATP and [Cho][Sal] molecules in water and in the mixture of these hydrotropes were investigated using Radial Distribution Functions (RDF). As expected, the ATP exhibited a self-aggregating tendency at a distance of 4-5 Å and up to 15 Å (Figure 2a). The self-aggregating propensity of ATP molecules from a chemical perspective in the presence of IL can occur in three possible ways, first the anion-π interactions between the aromatic ring and negatively charged oxygen moiety of phosphate groups, secondly a non-bonding aromatic ring interactions (H-bonding, π–π stacking interactions, and cation–π interactions) and third, H-bond formation between sugar and triphosphate group.[11] From the present analysis, it is evident that two of the ATPs preferentially formed stack-like configurations in water (Figure S1a). In presence of [Cho][Sal], the H-bonding mediated by IL (Figure S1b) markedly decreased the occurrence of the stack-like configurations of ATP molecules thereby increasing the multifacet nature of ATP self-aggregation (Figure 2a, blue color). Notably, indulgent of IL at the molecular concentration of 300mg/mL increases the H-bonding network mediated by cholinium or salicylate (Figure S1c). Unsurprisingly, we have not observed any perturbation of [Cho][Sal] nanostructure upon the addition of ATP, given its low concentration. In addition to RDFs, the self-aggregating behavior of ATP and ATP+IL was further verified by a concentration-dependent ζ-potential study (Figure 2c and Figure S2). At 1 mM concentration, which is below the critical hydrotropic concentration (2 mM), a single broad distribution peak was observed with maxima of -8.12 mV

indicating the existence of a single non-aggregated structure (Figure 2c). At 2.5 mM, the distribution curve shifted to a lower negative value with peak maxima -5.96 mV. This lowering in the ζ-potential indicates the beginning of aggregated structures similar to the self-aggregation of nanoparticles as a result of the decrease in the electrophoretic mobility.[28]

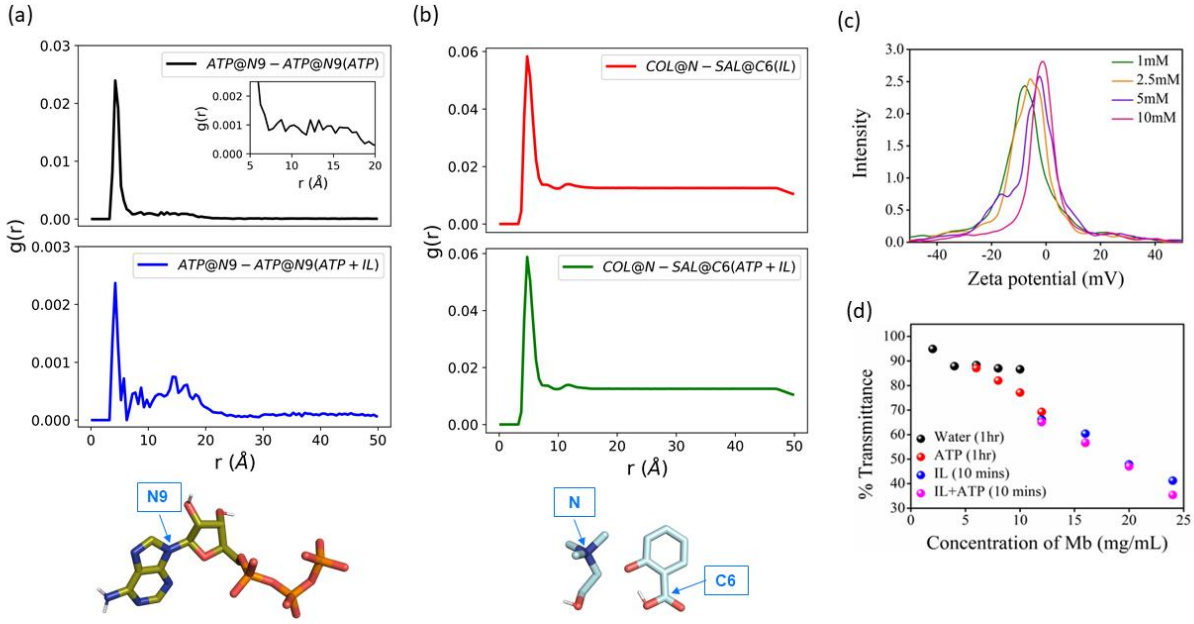

Figure 2: **Mutual effects of ATP and [Cho][Sal] on their respective nanostructure and interactions**. (a) Radial Distribution of Functions (RDF) of 5 mM ATP (black) and 5 mM ATP in presence of [Cho][Sal] (blue). The atom N9 of ATP used for RDF calculation is shown by the blue arrow. (b) RDF of 300 mg/mL [Cho][Sal] (red) and [Cho][Sal] with added ATP (green). The atoms N of and C6 used for RDF calculation are shown by blue arrow (c) Concentration-dependent Zeta potential analysis of ATP. (d) shows solubility data of equine heart myoglobin in an aqueous medium at pH 7 in the absence and presence of 5 mM ATP, 100 mg/mL [Cho][Sal], and a combination of both ATP+IL.

This is further evident by the shift of maxima from -5.96 to -2.35 mV for 5 mM ATP. Finally, at 10 mM concentration, a broad single peak with maxima at -1.42 mV was obtained which indicates the presence of a self-assembled nanostructured state of ATP. On the other hand, 200mg/mL of [Cho][Sal] shows a very broad Gaussian peak with a maximum at -9.12 mV (Figure S3), which in the presence of 5mM ATP, shifts to a lower value of -4.02 mV justifying the hypothesis of IL enhancing the self-assembly of amphiphiles.[19] The hydrodynamic radius (R_h) of 5 mM ATP was found to be 0.83 nm (a little higher than R_h of monomeric ATP, which is 0.57-0.65 nm)[10] which suggests the existence of nano-structured/oligomeric form and supports the earlier evidence. In the presence of IL, the R_h of ATP increased to 1.12 nm (Figure S4). To prove the hydrotropic property of ATP and [Cho][Sal], solubility studies of myoglobin (Mb) were carried out in an aqueous medium at pH 7 in the absence and presence of 5 mM ATP, 100 mg/mL IL and a combination of both (Figure 2d). After 1hr, the maximum solubility of Mb was found to be 6 mg/mL. In contrast, ATP-aided solubility of Mb increased to 16 mg/mL in the same duration, which directly shows the hydrotropic nature of ATP. In the case of [Cho][Sal], the same solubility was achieved within 5 mins. Thus, the concentration of Mb was further increased and studied till 24 mg/mL. Interestingly, for ATP+IL, 24 mg/mL Mb showed better solubility than only IL medium. This observation of enhanced solubility in the presence of two hydrotropes inspired towards nanoconfinement of Cyt c using ATP and [Cho][Sal]-based nanostructured hydrotropes envisaging improved biological activity and stability of the protein.

Structural features of nanostructured hydrotropes caged Cyt c

To understand the structural features of caged Cyt c, four molecular systems were prepared keeping Cyt c in water, ATP, IL, and both ATP + IL at 300 K (Figure 3a-d). The RDFs of hydrotropes in all systems without and with the presence of the protein were in good agreement, indicating that the presence of Cyt c had a negligible effect on nanostructures adopted by hydrotropes (Figure 2a,b & Figure S5). A lower dielectric constant of the protein or more negative zeta potential of ATP and IL can be related to the colloidal stability of caged Cyt C. Accordingly, ζ-potential analysis was employed to envisage the electrostatic interaction between Cyt c and nanostructured hydrotropes. ζ-potential of native Cyt c solution (10 μM) was found to be +1.24 mV (Figure 3e). ζ-potential of ATP (5 mM), IL (200 mg/mL), and ATP+IL was -2.48 mV, -9.16 mV, and -4.09 mV, respectively. After incubation of Cyt c with ATP, IL, and IL+ATP, the ζ-potential values decreased to -1.66 mV, -6.64 mV and -3.46 mV, respectively (Figure 3e). These changes in the ζ-potential demonstrate the possible electrostatic interaction between the protein and the nanostructured hydrotropes. At a lower concentration of

Cyt c (2 μM), the ζ-potential of ATP increased from -2.4 8mV to -4.38 mV indicating the reorganization of self-assembled ATP nanostructure around Cyt c (Figure S6). Further R_h of native Cyt c was found to be 1.25 nm, which agrees with the previous report,[30] and in the presence of ATP, the value increased to 1.99 nm showing self-assembly of ATP around the protein (Figure 3f and Figure S7). In the presence of IL+ATP, R_h of Cyt c is further increased to 2.22 nm. Thus, the hydrotropic mechanism of ATP occurs first by charge reinforcement, followed by the stacking phenomenon. Along with ζ-potential and DLS, structures of nanoconfined Cyt c were further characterized by UV-vis spectra (Figure S8). UV-Vis spectrum of pure Cyt c comprises a Soret (B-band), Q band, and a shoulder peak (N-band), altogether representing the structural morphology around the heme group (Figure S8). In the presence of 5mM ATP, a hyperchromic shift (a blue shift of 2 nm) in the Soret band (409 nm) was observed which suggested that a non-polar environment dominates around the heme. In the case of IL (300 mg/mL [Cho][Sal]), absorbance in the Soret band enhanced considerably along with a blue shift, and also Q-band (520-550 nm) is broadened due to enhanced absorbance. This gives the possibility of changes in the tertiary conformations. An additional broad peak can be seen in the range of 620-695 nm, the intensity of which increases with an increase in the concentration of IL, which accords with the local stability induced by [Cho][Sal].[31] Moreover, the observed peaks suggest that a transit towards penta co-ordinated Cyt c is formed in the presence of IL leading to the formation of a high-spin Fe(III) heme center.[31] Cyt c caged with both ATP and IL, a hypochromic shift in the Soret band region was observed, which indicates the stability offered by both the hydrotropic systems by driving the protein core towards the non-polar regime. Overall, as discussed above, it is evident that the self-aggregation propensities of the hydrotropes persisted even in the presence of Cyt c and the structure of caged Cyt c was partially affected (without any unfolding, as discussed below) due to multiple interactions with nanostructured hydrotropes

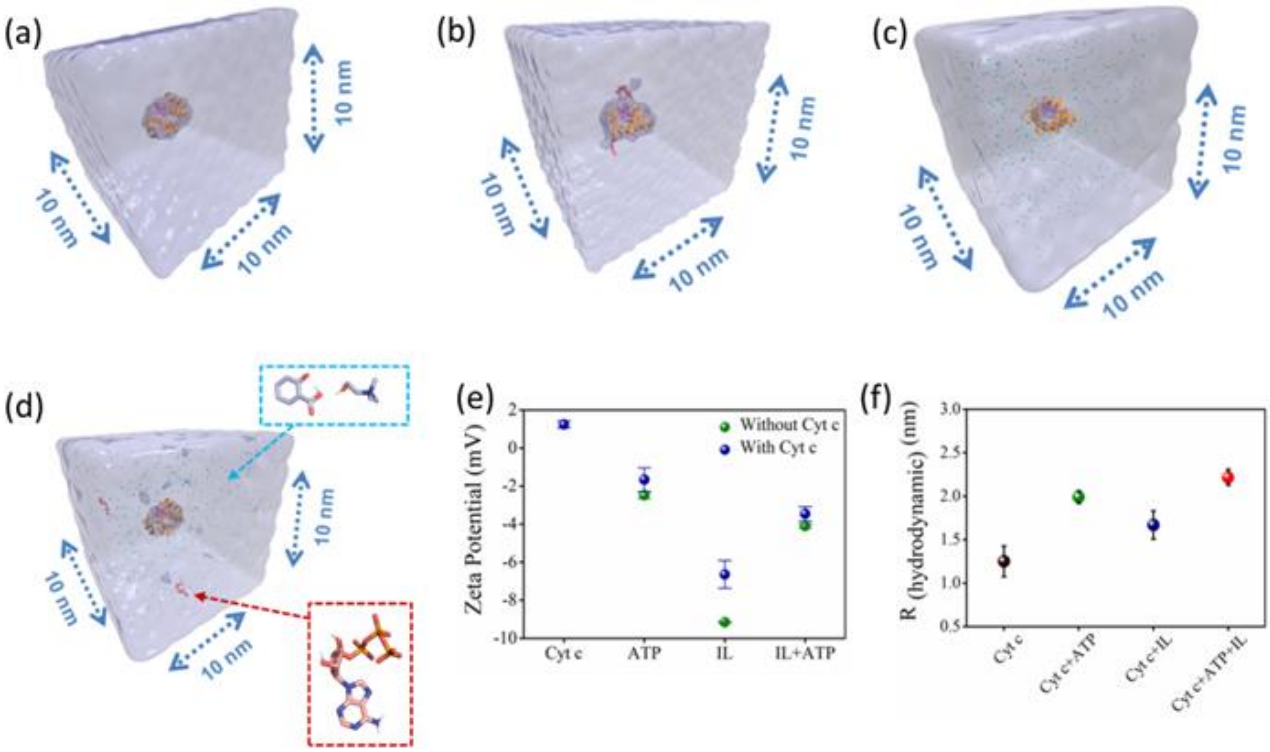

Figure 3: (a-d) Representative figures of a solvent of cubic box length 10 nm for Cyt c in H_2O (a), ATP+ H_2O (b), [Cho][Sal] + H_2O (c), and ATP + IL + H_2O molecular systems (d). Graph (e) shows zeta (ζ)-potential studies of nanostructured hydrotropes and Cyt c with and without nanostructured hydrotropes. Plot (f) depicts the hydrodynamic radius (R_h) of native Cyt c and Cyt c caged in different nanostructured hydrotropes

.

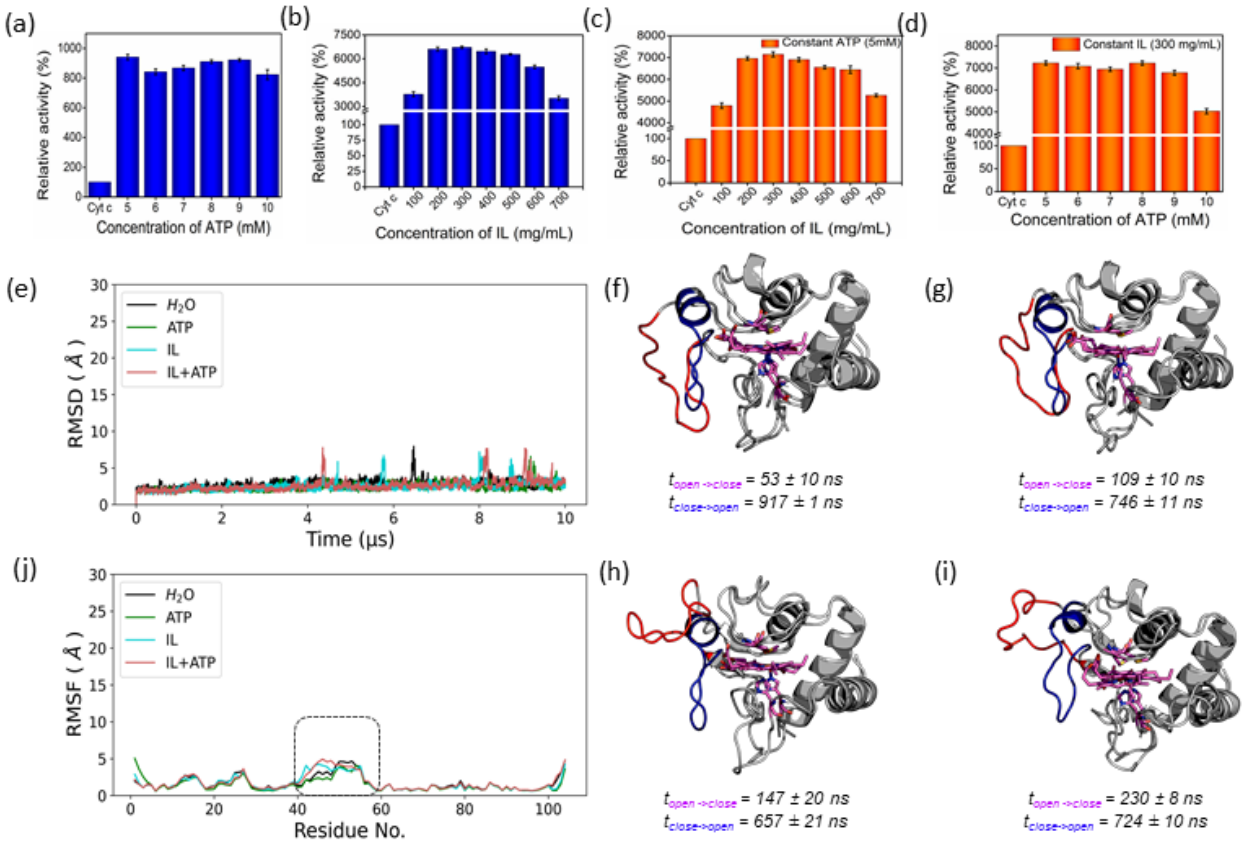

Figure 4: **Peroxidase-like activity of Cyt linked to its dynamics.** Optimization results of peroxidase-like activity of Cyt c with different hydrotropic concentrations of (a) ATP, (b) [Cho][Sal] IL, (c) varying [IL] by keeping [ATP] constant (5 mM), and (d) varying [ATP] by keeping IL constant (300 mg/mL). Structural characterization of Cyt c in four solvent systems at 300 K. (e) Stability and dynamics of Cyt c structure simulated in four solvent systems shown as backbone RMSD and RMSF, respectively. The peaks in the RMSD plot correspond to the reversible openings of region Ω 40-54 highlighted in the RMSF plot by a dashed rectangle. Figures (f-i) show the metastable states representing open (red) and closed (blue) structures of Cyt c in H_2O, ATP, IL, and ATP+IL, respectively. The timescales of opening and closing processes were calculated as mean first passage times between the two states presented as mean ± standard deviation.

Nanostructured hydrotropes caged Cyt c with boosted peroxidase activity: molecular insights on the improved catalytic activity and enhanced stability

In the presence of H_2O_2, Cyt c undergoes covalent modifications because of which it exhibits peroxidase-like activity.[32] The activity of Cyt c in the presence of 5-10 mM ATP showed a similar trend with >8-fold higher than native Cyt c (Figure 4a). Since a typical nanostructure is formed around Cyt c in the range of hydrotropic concentration (5-10 mM), similar relative activity is achieved rather than a maxima-minima trend. ATP acts as a hydrotrope first by unwinding the protein and then stabilizing the extended chain through electrostatic interactions,[11] which might be a reason for the high peroxidase activity. In the case of [Cho][Sal] IL, nearly the same relative activities were seen from 200 to 500 mg/mL range (Figure 4b). A clear trend was observed with the highest relative activity of 67-folds at the concentration of 300 mg/mL of IL. The activity data are in agreement with the UV-vis absorbance spectra that inferred the transition of Cyt c towards penta co-ordinated high spin complex. When Met_{80} ligand is displaced, Cyt c naturally exhibits pronounced peroxidase-like activity.[32] A replica of the IL optimization trend pattern was observed when ATP was kept constant (5mM) and IL was varied (Figure 4c). At 300 mg/mL IL and 5mM ATP concentration, the activity of the Cyt c was enhanced 72-folds than native Cyt c. This enhancement in the activity is indicative that the structure of Cyt c is still intact and combined hydrotropic systems boost the peroxidase activity further. Some ILs enhance the self-assembly of co-solutes in the media due to the virtue of their solvophobic effects.[17] Accordingly, the concentration of ATP was varied with IL being constant (300 mg/mL). A similar trend like only ATP was observed with >69 folds (Figure 4d). These trends demonstrated that both IL and ATP further enhance the changes in the conformation of Cyt c, followed by the stabilization of extended protein structure by the self-assembling of ATP around it. Similar inference can be observed from Figure S5a (blue line), ATP tends to self-aggregate even in the presence of IL and Cyt c.

To understand the behavior of nanostructured hydrotropes caged Cyt c, adaptive sampling MD simulations with a total of 10 µs simulation time for each system were performed. In all systems, we observed reversible structural rearrangements of the protein backbone (Figure 4e), which could be traced to the reversible opening of the loop in the Ω 40-54 region that was relatively more mobile than

other parts of the protein for all the four systems (Figure 4j). This region corresponds to mAb 1D3 binding site and is reported to be more dynamic,[33] while having specificity towards Cytochrome c oxidase.[34]

To delineate the details of this process and its modulation by the action of nanostructured hydrotropes, we have constructed Bayesian Markov state models from the simulations. This inference revealed the presence of metastable states with an open conformation of the Ω 40-54 loop of Cyt c in all systems (Figures 4f,g,h,i), which were characterized by their increased RMSD and elevated radius of gyration (Figure S9). The interactions of ATP and IL with Cyt c resulted in marked effects on the stability and dynamics of this region. In the presence of ATP, the closing process was about twice slower, whereas the opening became almost 20 % faster (Figure 4g). Similarly, the presence of IL resulted in a speed-up of the opening process and slowed down closing even more prominent than in the case of ATP (Figure 4h). Finally, the mixture of ATP and IL showed a synergistic effect on the dynamics of Cyt c, resulting in the slowest closing and faster opening in contrast to the water environment, enhancing the functional dynamics of this functionally important region (Figure 4i).

Since both ATP and IL were significantly affecting the dynamics of Cyt c, the residues exhibiting the most frequent H-bonding with hydrotropes were identified from the simulations (Figure 5a-c).In general, ATP interacted preferably with Lys residues (Figure S10a), which is in accordance with an earlier report that ATP can deliver weak non-specific interactions with conserved Lys or Arg with the triphosphate group.[10] Additionally, IL had a wide range of residues for binding partners but, here too, Lys was the most populated in terms of H-bonding (Figure S10b). Such a trend was also maintained in the mixture of ATP and IL (Figure S10c).

We observed marked overlap in particular interaction hotspots for IL and ATP on Cyp c surface (Figure 5a-c, Figure S10d,e). The ATP formed most often interactions with K13, K25, K27, K72, K86, and K87 (Figure S11a,c). Notably, K72 is involved in site A of Cyt c which is crucial for interacting with cardiolipin,[35] and was reported to have a significant role in peroxidase activity of Cyt c.[36] Conversely, IL had shown the highest affinity towards Y97 (Figure S11b,d) despite its general preference to Lys. Interestingly Y97 has been ascribed a significant role in keeping the terminal helix intact and hence providing structural stability to the protein.[37] Finally, these simulations also revealed variation in the secondary structures of native Cyt c and caged Cyt c in the presence of IL, where the transition of turn to parallel beta-sheets was observed (Figure 5d).

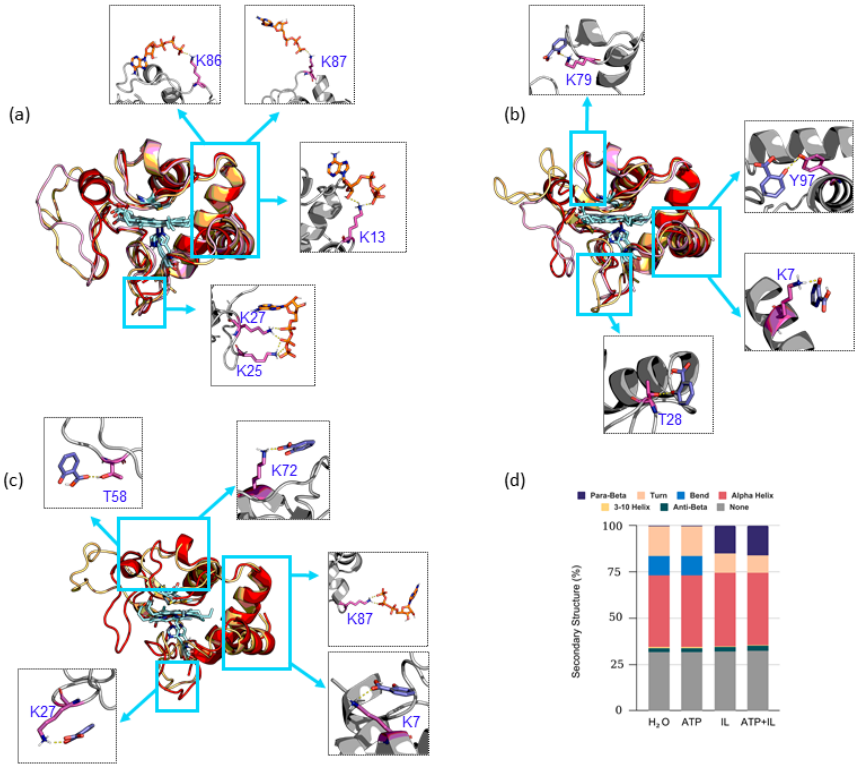

Figure 5: Interaction of hydrotrope molecules in metastable states in the open, closed, and transient conformations of Cyt c from 10 μs adaptive simulation data with (a) ATP, (b) [Cho][Sal] IL, and (c) ATP + IL. The top residues having hydrogen bond interactions between solvent molecules and Cyt c are shown in gray squares (dashed), and the regions of the protein are highlighted in cyan (solid). Plot (d) shows secondary structural changes for the four Cyt c systems generated. All simulations were performed at 300 K. In all cases, the concentration of ATP and IL was 5 mM and 300 mg/mL, respectively.

Nanostructured hydrotropes caged Cyt c with enhanced thermal stability for high-temperature biocatalysis

Figure 6a shows the temperature-dependent activity of Cyt c in the presence of nanostructured hydrotropes. The activity of Cyt c increases with temperature up to 70 °C, above which the protein starts to denature gradually. Above 80 °C, the activity drops due to significant denaturation of the protein.[25] The similar trend is obtained in the presence of ATP, but the activity extends to ~20 folds than native Cyt c at 70 °C. In the case of IL and IL+ATP systems, the denaturation is prevented even up to extremes of 110 °C. At 90 °C, both Cyt c+IL and Cyt c+IL+ATP showed an accelerated activity value corresponding to 76-80-folds than the native Cyt c. The stability aspects of Cyt c with hydrotropes at elevated temperatures were backed by UV-vis spectra (Figure 6b). Enhancement in the Soret band intensity was observed in the case of IL and IL+ATP at 90 °C compared to the results obtained at 300 K, which implies that the secondary conformation formed due to weak interactions between the hydrotrope systems and the Cyt c was preserved. ATP+IL showed intensified Soret peak compared to the rest at 110 °C suggesting the advantage of engineering Cyt c with two different hydrotropes aiming for high-temperature biocatalysis. Additionally, as evident from non-reducing SDS-PAGE (Figure 6c), improved activity trends at high temperatures were achieved without structural degradation of the protein.

A systematic computational study was undertaken to infer structural insights into the higher stability of nanostructured caged Cyt c at elevated temperature (363.15 K). As expected, Cyt c conformational ensemble was notably altered at the higher temperature with backbone RMSD being about 3-4 times higher than that of at 300K in all four solvents(Figure S12a). No significant effects were observed between the mobility of the region Ω 40-54 in four systems than that observed for 300K (Figure 4e and S12b). However, the thermal stability of Ω 70-85 region was significantly enhanced with nanostructured hydrotropes than neat water systems (Figure S12b). From Bayesian Markov state models constructed based on the high-temperature simulations (Figure S12c-f), we could observe that Cyt c in water exhibited severe conformational instability, underlined by a very high RMSD of the open state, as well as the presence of multiple secondary open-like states (Figure S13). In contrast, the presence of ATP or/and IL restricted the maximal range of the Cyt c backbone displacements, providing resistance of Cyt c to heightened. Notably, IL stabilized Cyt c in its closed state, particularly when mixed with APT (Figure S13). Hence, it is evident that ATP and IL could thermally stabilize the functional part of Cyt c via multiple polar interactions.[24] Affinity of hydrotropes molecules towards specific amino acids at the higher temperature (Figures 6d-h and Figure S14) were found to be similar to that observed at 300K (Figures S14 & S11). Overall, Lys and Arg were found to have frequent H-bonding at 363.15K to ATP (Figures 6d, f,g). Similarly to the lower temperature, IL had a broader range of specificity having more affinity with Lys and Tyr in terms of H-bonding (Figures 6e,f,h). The highest affinity was seen towards K8, K13, R38, K39, K73, K86, and K87 with ATP (Figure 6h), and K13, R38, Y67 , T78, and K79 with IL (Figure 6i), which are very crucial in maintaining thermal stability.[38]

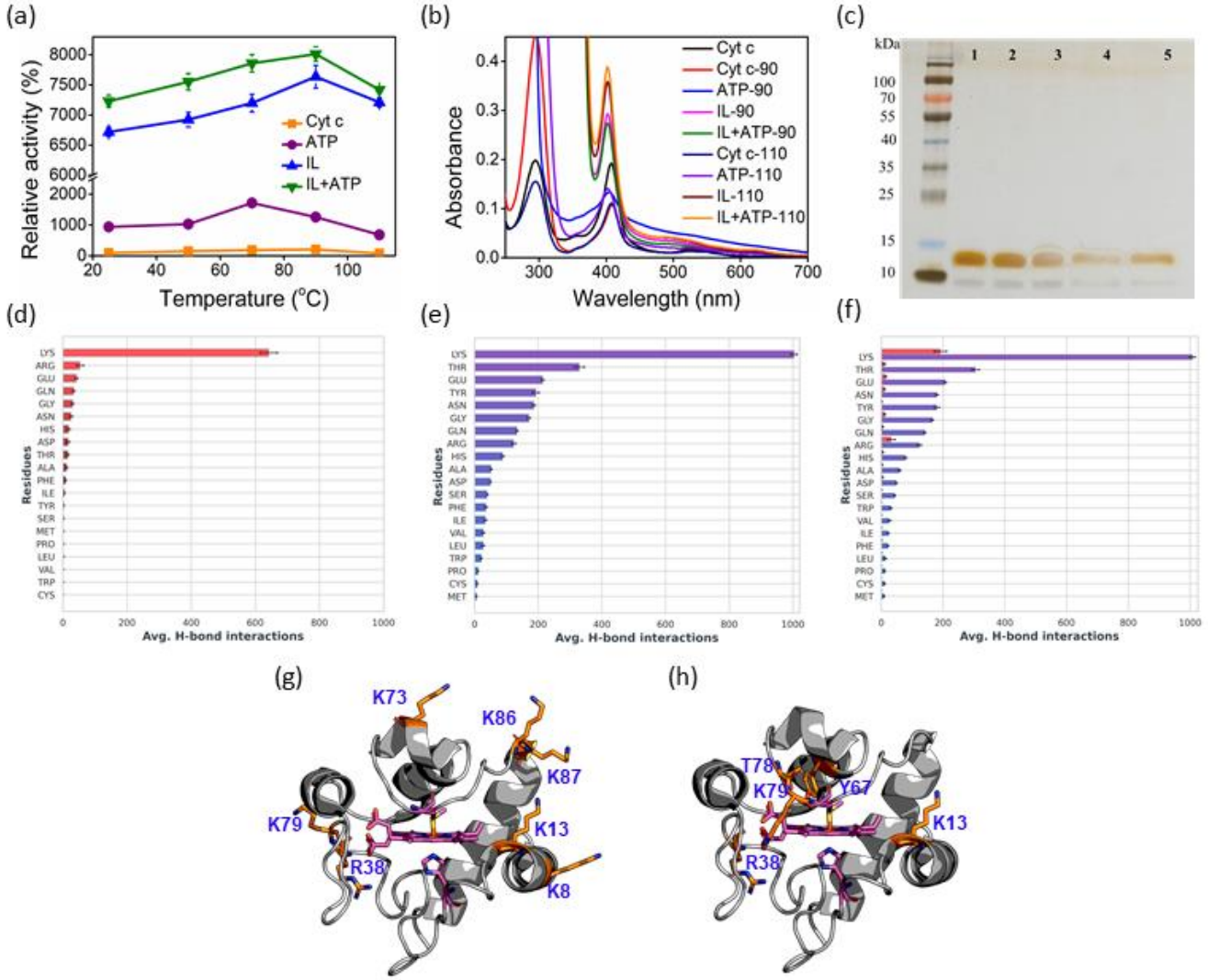

Figure 6: (a) Peroxidase activity of Cyt c with and without nanostructured hydrotropes at different temperatures. (b) UV-vis spectra of Cyt c at higher temperatures (90 °C and 110 °C) with and without nanostructured hydrotropes. (c) SDS-PAGE image of native Cyt c (lane 1), Cyt c incubated at 100 °C (lane 2), Cyt c + ATP incubated at 100 °C (lane 3), Cyt c + [Cho][Sal] incubated at 100 °C (lane 4), and Cyt C + ATP + [Cho][Sal] incubated at 100 °C (lane 5). (d-f) H-bonding interaction counts of individual residue types obtained from adaptive simulation data of Cyt c in the presence of ATP (d), IL (e), ATP and IL in ATP+IL system (f) are depicted with ATP in red and IL in blue. All simulations were performed at 363.15 K. Plot (g, h) depicts the position of residues having a higher occurrence of H-bonding with ATP (g) and IL (h), respectively. In all cases, the concentration of ATP and IL was 5 mM and 300 mg/mL, respectively.

Improved stability of nanostructured hydrotropes caged Cyt c against chemical denaturants

Above a particular concentration and on more prolonged exposure to some chaotropic chemicals like H_2O_2, guanidine hydrochloride (GuHCl), and urea cause the amide bond disruption or overexposes the metallo-core of the enzyme, because of which the enzyme loses the structural integrity and its function. To shield the Cyt c against such chemical denaturants, the protein was incubated with the three nanostructured hydrotropic systems for 10 mins, followed by the addition of a respective chemical denaturant. After the interaction with 6 M GuHCl for 15 mins, there was a complete disruption in the heme pocket of the native Cyt c and the activity was severely declined with the remaining activity of ~20%. Whereas hydrotropes caged Cyt c maintained their initial activity of 8.5-fold, 63-fold and 66-fold in the presence of ATP, IL and ATP+IL, respectively (Figure 7a). Urea is known to be a hydrotrope but at the same time, it is well recognized as a chemical denaturant above the concentration 6 M. In the pre-denaturation concentrations of urea (1-6M), ~30 folds increase in peroxidase-like activity was obtained for Cyt c.[39] After 30 minutes incubation at 8 M urea concentration, 70% remaining activity of Cyt c was recorded, while IL and ATP+IL hydrotrope stabilized Cyt c showed similar activity (Figure 7b). In the UV-vis spectra with GuHCl (Figure 7c), native Cyt c shows denaturing pattern where the Q band structure is entirely lost and the Soret band is severely blue-shifted. In the case of ATP, changes in the 280 nm shoulder peak suggest partial dissociation of aromatic residues like Tyr and Trp. In contrast, in the case of IL and ATP+IL, the structures remained almost the same except that absorbance of the IL-based system was slightly lowered. In the case of ATP, the activity of

Cyt c almost doubled (~24 folds than native Cyt c) in the presence of urea compared to Cyt c+ATP system (Figure 7b). This strange observation suggested that ATP cannot prevent the further unfolding of Cyt c in the presence of urea. This behavior was confirmed by UV-vis spectra. For only Cyt c, a blue shift similar to GuHCl along with disruption of the Q band was observed, but for Cyt c-ATP system, the Q band was retained. The hypochromic shift in the Soret peak in Cyt c-ATP indicated the beginning of structural deformation. IL and ATP+IL followed the regular trend and the lower activity can be envisioned by the lowering of the Soret peak intensity (Figure S15). Further, SDS-PAGE analysis showed that Cyt C did not degrade by denaturing agent treatment with and without the presence of ATP and [Cho][Sal] (Figure 7d), thus, confirming that the variation in the activity was due to the changes in the structural conformation of the protein.

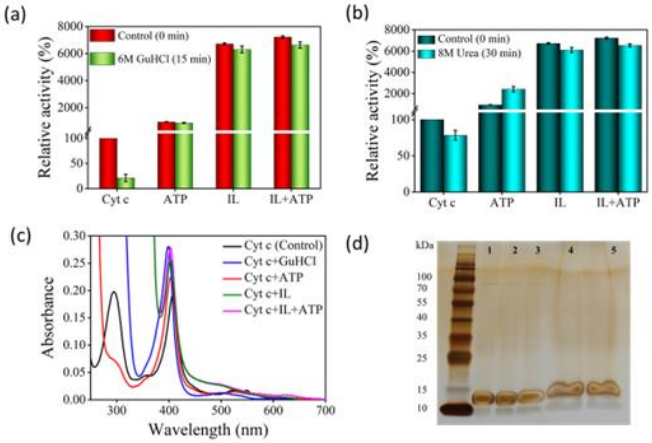

Figure 7: Effect of chemical denaturants, 6 M GuHCl (a) and 8 M urea (b) on the peroxidase activity of Cyt c and nanostructured hydrotropes caged Cyt c. (c) UV-vis spectra of Cyt c after incubation with 6 M GuHCl. (d) SDS-PAGE image of native Cyt c (lane 1), Cyt c incubated with 8 M urea (lane 2), Cyt c + ATP incubated with 8 M urea (lane 3), Cyt c + [Cho][Sal] incubated with 8 M urea (lane 4), and Cyt C + ATP + [Cho][Sal] incubated with 8 M urea (lane 5). In all cases, concentration of ATP and IL was 5 mM and 300 mg/mL, respectively.

Nanostructured hydrotropes caged Cyt c against protease digestion

Trypsin being a proteolytic enzyme hydrolyses the peptide bond particularly at basic amino acids like Arg and Lys residues (Figure 8a), thereby denaturing the protein/other enzymes.[40] Native and hydrotropes stabilized Cyt c systems were incubated with 6 μM trypsin at 37 °C for 24hr. After the interaction, only 25% of activity was retained in native Cyt c, whereas the hydrotropic systems showed excellent performance in keeping the Cyt c safe from trypsin action (Figure 8b). Cyt c in presence of ATP lost only ~2 folds activity compared to activity at 0th hour (~700% retained), whereas IL and ATP+IL systems retained ~61 and ~67 folds relative activity, respectively. This excellent performance against protease digestion can be deduced by looking closely at the interactions of ATP and IL with Cyt c. H-bonding analysis revealed that ATP has a higher tendency to interact with Lys, Arg, and Gln more prominently at both 300 K and 363.15 K temperatures, thus, suggesting the efficacy of ATP to impart stability to Cyt c (Figure S12 and Figures 6d-6g). Additionally, IL also greatly affected the dynamics nature by interacting with a wide range of residues. The affinity of ATP and IL towards Lys and Tyr may be helpful to protect Cyt c by hindering the trypsin degradation mechanism. The electrostatic and H-bonding interactions of ATP followed by nano-structuring completely safeguard the protein from the action of trypsin (Figure 8a). This was further proved by non-reducing SDS-PAGE analysis of the Cyt c before and after digestion with trypsin (Figure 8c). Most of the native Cyt c in presence of trypsin was found degraded (lane 2, Figure 8c). However, the protein was significantly intact when it was digested in the presence of ATP, IL and both. From UV-vis spectra (Figure S16), it can be seen that the Q band is lost in almost all the cases (except with ATP) after incubation with trypsin, however, only marginal changes were observed in the Soret band of Cyt c+ATP, and Cyt c+ATP+IL systems, indicating the stability induced by the nanostructured hydrotropes.

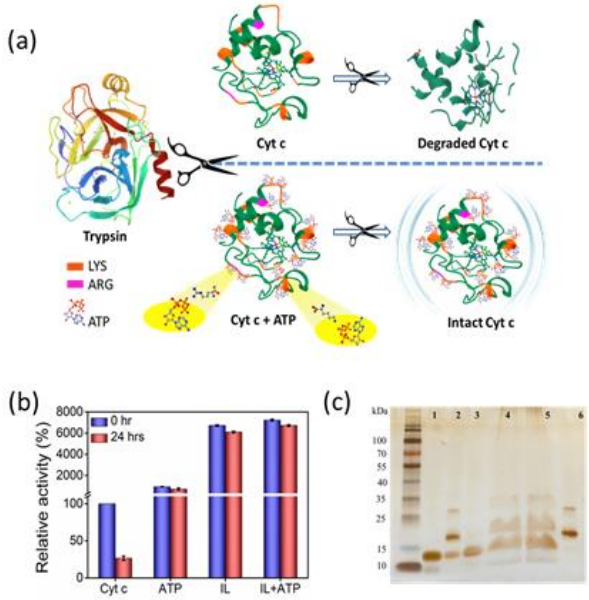

Figure 8: (a) Plausible mechanism of Cyt c digestion in the presence and absence of nanostructured hydrotropes. (b) Effect of protease digestion (6 μM trypsin) of peroxidase activity of Cyt c. (e) SDS-PAGE image of native Cyt c (lane 1), Cyt c incubated with trypsin (lane 2), Cyt c + ATP incubated with trypsin (lane 3), Cyt c + [Cho][Sal] incubated with trypsin (lane 4), Cyt C + ATP + [Cho][Sal] incubated with trypsin (lane 5), only trypsin (lane 6). In all cases concentration of ATP and IL was 5mM and 300 mg/mL, respectively.

Nanostructured hydrotropes caged Cyt c against oxidative stress

Unlike other stress conditions where the peptide backbone is attacked, H_2O_2 targets the catalytic site first, followed by a breakdown of peptide bonds. Thus, H_2O_2 even after being essential for the peroxidase activity of Cyt c, on prolonged exposure, causes severe impairment in the protein structure.

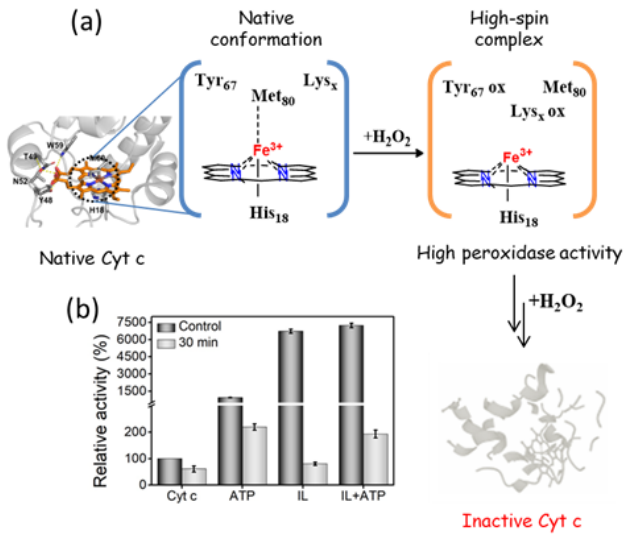

Figure 9: (a) Schematics mechanism showing H_2O_2 induced structural degradation of Cyt c. (b) Effect of H_2O_2 on the peroxidase activity of Cyt c in the presence of different hydrotropes.

In the rest of the earlier activity studies, 1 mM of H_2O_2 was added at last, whereas for this study, Cyt c is incubated with H_2O_2 for 30 mins and the substrate is added after that. The activity of bare Cyt c after the induced oxidative stress was found to be only ~60% of its original activity, whereas, in the presence of ATP, ~219% activity was retained. This observation can be correlated with the earlier findings where ATP was found to prevent the oxidation of Cyt c from Cyt c oxidase enzyme in the mitochondria but by hampering the electron flow rate.[41-42] On the other hand, there was a severe drop in the activity of Cyt c from 6700% to just 80% in the presence of IL. These results are not astonishing since the salicylate counterpart is known to enhance the formation rate of reactive oxygen species (ROS).[22] However, the presence of ATP is found to prevent the oxidation and Cyt c from IL-induced oxidative stress and showed 192% relative activity. These findings clearly demonstrate the stabilizing effect of nanostructured ATP around Cyt c.

CONCLUSIONS

In summary, this study systematically demonstrated the robustness of ATP and IL-based mixed nanostructured hydrotropes having utility towards improved protein packaging in extreme conditions. From the solubility data of Mb, it was shown that the hydrotropic nature of ATP accelerated with the addition of a co-hydrotrope like [Cho][Sal] and vice-versa. Through RDF, DLS, ζ-potential, and UV-vis data, it was convincing that ATP forms oligomeric nanostructures above the concentration of 2.5 mM around Cyt c, which can be augmented further with the addition of [Cho][Sal]. A 9-fold increase in peroxidase activity with ATP, 67-fold with IL, and 72-fold with IL+ATP suggested a 'partial reversible unfolding-electrostatic stabilization' mechanism. Reversible binding of ATP and IL with Ω 40-54 loop region of Cyt c proved the higher stability at 300 K. Whereas, specific binding of nanostructured hydrotropes with Cyt c to Lys and Arg through H-bonding and polar interactions with Ω 70-85 region presented an exceptionally high thermal tolerance with 80-folds activity even at 363.15 K. Because of such binding specificity, the structure and activity of nanoconfined Cyt c were found to be retained against protease digestion, which cleaves explicitly at Lys and Arg residues. Further, ATP and IL-based nanostructured hydrotropes showed efficacy in retaining the functional integrity of Cyt c even in the presence of chemical denaturants like urea and GuHCl, which suggested the suitability of such solvent manipulation strategy to expand industrial biocatalysis. Through oxidative stress studies, a stark observation was made where [Cho][Sal] was found to enhance the ROS formation which could be efficiently tackled by adding ATP. These results can open the door for counteracting oxidative stress inside the living cells. Thus, the novel strategy of protein confinement in nanostructured hydrotropes can find significant usage in protein packaging under biotic and abiotic stresses, high-temperature biocatalysis, and plant cell protection against ROS.

EXPERIMENTAL SECTION

Materials and characterization techniques, ionic liquid synthesis, solubility study of Mb, and SDS-PAGE analysis details are provided in supporting information.

Peroxidase activity of Cyt c at room temperature and under harsh conditions: For activity profiling, a standard ABTS assay was employed where ABTS (3 mM) is oxidized to $ABTS^{+\bullet}$ in presence of H_2O_2 (1 mM) catalyzed by Cyt c (2μM). All the chemicals were kept at 25 °C for an hour followed by the interaction of Cyt c with different concentrations of ATP, IL and IL+ATP for 10 minutes. With the addition of ABTS and peroxide, the green colour of ABTS intensifies due to the formation of cationic radical, and variation of absorbance at 420 nm was monitored for 60 seconds with 1 sec interval, resulting in a straight line. For temperature studies, Cyt c alone and the ones incubated with hydrotropic systems were allowed to attain room temperature after subsequent heating (from 25-110 °C for 30 mins). For chemical denaturants, 8M of urea and 6M of

GuHCl were added to the native and pre-incubated catalytic systems and the activity was checked at 30th and 15th min, respectively. For profiling the activity of Cyt c in presence of biological denaturant, native protein and the Cyt c with hydrotropes were further incubated with 6μM of trypsin at 37 °C for 24 hrs and finally for oxidative stress, all the systems were kept for reaction with H_2O_2 first (for 15 mins) followed by the addition of ABTS. For all the activity studies, the slope of the curve obtained for native Cyt c was taken as 100% and the activity of other systems was calculated relative to this.

***System setup and Molecular Dynamics simulation*:** The input model was based on the crystallographic structure of bovine heart Cyt c (PDB code: 2B4Z) at 1.5Å resolution. The force field parameters for the heme cofactor were referred from literature for which the geometry optimization was done using Gaussian 16 program.[43] All the simulations were set up using AMBER 18 platform.[44] The parameters for ATP were retrieved from AMBER parameter database.[45] Structures of [Cho][Sal] were obtained from PubChem database (CID 54686350) and the force field parameters were generated using the Antechamber program and General Amber Force Field - GAFF2 charges.[46-47] Four molecular systems were prepared keeping the protein cytochrome c in water, ATP, ionic liquid (IL) and both ATP and IL. All molecular systems were solvated in a cubic box of length 10 nm box side length prepared using a PACKMOL package.[29] The number of ATP molecules corresponds to the concentration of 5 mM which is 3 ATP molecules and the number of IL corresponds to 300 mg/mL with a total of 350 molecules of [Cho][Sal]. The protein was modeled using the AMBER ff19SB force field.[48] The protein structure was further protonated using H++ web server pH 6.8.[49] The protein complexes were solvated using OPC water models and then neutralized with counter ions (Na^+ and Cl^-) to achieve the ionic strength of 0.1M. The systems were then minimized using PMEMD and PMEMD.CUDA modules[50] of AMBER18 and equilibrated under constant pressure and temperature (NPT) conditions at 1 atm and 300 K using the Langevin thermostat and periodic boundary conditions using particle mesh Ewald method[51] with 4 fs time-step enabled by SHAKE and hydrogen mass repartitioning algorithms.[52] Using the steepest descent minimization method the systems were minimized for several rounds with decreasing harmonic restraints. The following steps included continued heating of the systems from 200K to 300K with restraints only on the heavy atoms for 1 ns followed by NPT equilibration with backbone restraints for 1 ns. Finally, the production run was performed using several rounds of unrestrained NPT simulations with a frame saving rate of 200 ps and total sampling time of 1 ns at constant temperature and pressure using the weak-coupling barostat and thermostat.[53] The final configurations of protein in different solvent environments were adopted for simulations at room temperature (300 K) and higher temperature (363.15 K). The last snapshots from the production run were used for the initial input structure for adaptive sampling simulations using the High-Throughput Molecular Dynamics (HTMD) package.[54] The dihedral angle of the protein backbone was defined as the guiding matrix in adaptive sampling simulations. A total of 10 epochs and each epoch consisting of 10 individual simulations of length 100 ns totaling 10 μs were sampled. All the trajectories were analyzed using the cpptraj program and its Python front-end, pytraj.[55] Further classical MD of 200 ns lengths were performed for solvents systems of ATP, IL, and both ATP and IL without protein.

***Markov state models*:** The Markov state models (MSM) were obtained using the functionalities of pyEMMA program implemented in HTMD protocol.[56] The high dimensionality space was reduced using time-lagged independent component analysis (TICA). The models were generated and the number of metastable states was selected based on the spectral separations analysis (Figures S17 & S18). Here lag time of 40 ns was chosen to estimate the final Markov model (Figures S19 & S20).

ASSOCIATED CONTENT

Supporting Information- Details of materials and methods, experimental processes, and figures related to DLS, zeta potential, UV-vis, and computational results have been provided. "This material is available free of charge via the Internet at http://pubs.acs.org." The parameters and input files for MD simulations variants, the key restart files, representative conformations of metastable states, and raw outputs from analyses, are freely available at https://doi.org/10.5281/zenodo.7602239.

AUTHOR INFORMATION

Corresponding Authors

GF: fgre@igr.poznan.pl
JB: janbre@amu.edu.pl; jbrezovsky@iimcb.gov.pl
DM: dmtapu@gmail.com; dmon@igr.poznan.pl

ACKNOWLEDGMENT

D.M. acknowledges SERB, India (EEQ/2021/000059), for the research grant. D.K.S. was a recipient of a scholarship provided by POWER project POWR.03.02.00-00-I006/17. The computations were performed at the Poznan Supercomputing and Networking Center. D.M. and G.F. acknowledge the NANOPLANT project, which received funding from the European Union's Horizon 2020 research and innovation program under grant agreement no. 856961.

REFERENCES

1. Eguchi, Y.; Srinivasan, A.; Tomaselli, K. J.; Shimizu, S.; Tsujimoto, Y. ATP-dependent steps in apoptotic signal transduction. *Cancer Res.* **1999**, *59*, 2174.
2. Fyodorov, D. V.; Kadonaga, J. T. Dynamics of ATP-dependent chromatin assembly by ACF. *Nature.* **2002**, *418*, 896.

3. Hochstrasser, M.; Wang, J. Unraveling the means to the end in ATP-dependent proteases. *Nat. Struct. Biol.* **2001**, *8*, 294.
4. Lee, S.-J. α-Synuclein aggregation: a link between mitochondrial defects and Parkinson's disease? *Antioxid. Redox Signal.* **2003**, *5*, 337.
5. Patel, A.; Malinovska, L.; Saha, S.; Wang, J.; Alberti, S.; Krishnan, Y.; Hyman, A. A. ATP as a biological hydrotrope. *Science.* **2017**, *356*, 753.
6. Neuberg, C. Hydrotropy. *Biochem. Z.* **1916**, *76*, 107.
7. Werner, K.; Krister, H.; Thomas, Z. Hydrotropes. *Curr. Opin. Colloid Interface Sci.* **2016**, *22*, 99.
8. Mei, D.; Jian, K.; Liangzhong, L.; Yifan, L.; Lu, W.; Jianxing, S. ATP is a cryptic binder of TDP-43 RRM domains to enhance stability and inhibit ALS/AD-associated fibrillation. *Biochem. Biophys. Res. Commun.* **2020**, *522*, 247.
9. Jack, V. G.; Thomas, G. Hydrotropic function of ATP in the crystalline lens. *Exp. Eye Res.* **2020**, *190*, 107862.
10. Nishizawa, M.; Walinda, E.; Morimoto, D.; Kohn, B.; Scheler, U.; Shirakawa, M.; Sugase, K. Effects of weak nonspecific interactions with ATP on proteins. *J. Am. Chem. Soc.* **2021**, *143*, 11982.
11. Sarkar, S.; Mondal, J. Mechanistic Insights on ATP's Role as a Hydrotrope. *J. Phys. Chem. B.* **2021**, *125*, 7717.
12. Johannes, M.; Tuan-Minh, D.; Didier, T.; Max, H.; Ali, K.; Dominik, H.; Werner, K. Hofmeister versus Neuberg: is ATP really a biological hydrotrope? *Cell Rep. Phys. Sci.* **2021**, *2*, 100343.
13. Ou, X.; Lao, Y.; Xu, J.; Wutthinitikornkit, Y.; Shi, R.; Chen, X.; Li, J. ATP Can Efficiently Stabilize Protein through a Unique Mechanism. *JACS Au.* **2021**, *1*, 1766.
14. Jiang, H. J.; Atkin, R.; Warr, G. G. Nanostructured ionic liquids and their solutions: Recent advances and emerging challenges. *Curr. Opin. Green Sustain. Chem.* **2018**, *12*, 27.
15. Sindhu, A.; Kumar, S.; Mondal, D.; Bahadur, I.; Venkatesu, P. Protein packaging in ionic liquid mixtures: an eco-friendly approach towards the improved stability of β-lactoglobulin in cholinium-based mixed ionic liquids. *Phys. Chem. Chem. Phys.* **2020**, *22*, 14811.
16. Sintra, T. E.; Abranches, D. O.; Benfica, J.; Soares, B. P.; Ventura, S. P. M.; Coutinho, J. A. P. Cholinium-based ionic liquids as bioinspired hydrotropes to tackle solubility challenges in drug formulation. *Eur. J. Pharm. Biopharm.* **2021**, *164*, 86.
17. Greaves, T. L.; Drummond, C. J. Solvent nanostructure, the solvophobic effect and amphiphile self-assembly in ionic liquids. *Chem. Soc. Rev.* **2013**, *42*, 1096.
18. Bui-Le, L.; Clarke, C. J.; Bröhl, A.; Brogan, A. P. S.; Arpino, J. A. J.; Polizzi, K. M.; Hallett, J. P. Revealing the complexity of ionic liquid–protein interactions through a multi-technique investigation. *Commun. Chem.* **2020**, *3*, 55.
19. Hayes, R.; Warr, G. G.; Atkin, R. Structure and nanostructure in ionic liquids. *Chem. Rev.* **2015**, *115*, 6357.
20. Sanchez-Fernandez, A.; Leung, A. E.; Kelley, E. G.; Jackson, A. J. Complex by design: Hydrotrope-induced micellar growth in deep eutectic solvents. *J. Colloid Interface Sci.* **2021**, *581*, 292.
21. Xie, Z.; Chen, Z. Salicylic acid induces rapid inhibition of mitochondrial electron transport and oxidative phosphorylation in tobacco cells. *Plant Physiol.* **1999**, *120*, 217.
22. Poór, P. Effects of salicylic acid on the metabolism of mitochondrial reactive oxygen species in plants. *Biomolecules.* **2020**, *10*, 341.
23. Martínez-Reyes, I.; Chandel, N. S. Mitochondrial TCA cycle metabolites control physiology and disease. *Nat. Commun.* **2020**, *11*, 102.
24. Alvarez-Paggi, D.; Hannibal, L.; Castro, M. A.; Oviedo-Rouco, S.; Demicheli, V.; Tórtora, V.; Tomasina, F.; Radi, R.; Murgida, D. H. Multifunctional cytochrome c: learning new tricks from an old dog. *Chem. Rev.* **2017**, *117*, 13382.
25. Shet, S. M.; Bharadwaj, P.; Bisht, M.; Pereira, M. M.; Thayallath, S. K.; Lokesh, V.; Franklin, G.; Kotrappanavar, N. S.; Mondal, D. Presenting B-DNA as macromolecular crowding agent to improve efficacy of cytochrome c under various stresses. *Int. J. Biol. Macromol.* **2022**, *215*, 184.
26. Chen, Y.; Jiménez-Ángeles, F.; Qiao, B.; Krzyaniak, M. D.; Sha, F.; Kato, S.; Gong, X.; Buru, C. T.; Chen, Z.; Zhang, X.; Gianneschi, N. C.; Wasielewski, M. R.; Olvera de la Cruz, M.; Farha, O. K. Insights into the enhanced catalytic activity of cytochrome c when encapsulated in a metal–organic framework. *J. Am. Chem. Soc.* **2020**, *142*, 18576.
27. Shet, S. M.; Thayallath, S. K.; Bisht, M.; Pereira, M. M.; Coutinho, J. A. P.; Sanna Kotrappanavar, N.; Mondal, D. Engineering, Engineering cytochrome c with quantum dots and ionic liquids: A win-win strategy for protein packaging against multiple stresses. *ACS Sustain. Chem. Eng.* **2021**, *9*, 8327.
28. Aurora, M.; Ileana, C.; Gheorghe, T.; Liviu-Dorel, B.; Ossi, H.; Maria, T.-C. Self-assembly characteristics of gold nanoparticles in the presence of cysteine. *Colloids Surf. A Physicochem. Eng.* **2009**, *338*, 93.
29. Allouche, A.-R. Gabedit—A graphical user interface for computational chemistry softwares. *J. Comput. Chem.* **2011**, *32*, 174.
30. Gomes, I.; Santos, N. C.; Oliveira, L. M. A.; Quintas, A.; Eaton, P.; Pereira, E.; Franco, R. Probing surface properties of cytochrome c at Au bionanoconjugates. *J. Phys. Chem. C.* **2008**, *112*, 16340.
31. Singh, U. K.; Kumari, M.; Khan, S. H.; Bohidar, H. B.; Patel, R. Engineering, Mechanism and dynamics of long-term stability of cytochrome c conferred by long-chain imidazolium ionic liquids at low concentration. *ACS Sustain. Chem. Eng.* **2018**, *6*, 803.
32. Yin, V.; Shaw, G. S.; Konermann, L. Cytochrome c as a peroxidase: activation of the precatalytic native state by H2O2-induced covalent modifications. *J. Am. Chem. Soc.* **2017**, *139*, 15701.
33. Kagan, V. E.; Tyurin, V. A.; Jiang, J.; Tyurina, Y. Y.; Ritov, V. B.; Amoscato, A. A.; Osipov, A. N.; Belikova, N. A.; Kapralov, A. A.; Kini, V.; Vlasova, I. I.; Zhao, Q.; Zou, M.; Di, P.; Svistunenko, D. A.; Kurnikov, I. V.; Borisenko, G. G. Cytochrome c acts as a cardiolipin oxygenase required for release of proapoptotic factors. *Nat. Chem. Biol.* **2005**, *1*, 223.
34. Bushnell, G. W.; Louie, G. V.; Brayer, G. D. High-resolution three-dimensional structure of horse heart cytochrome c. *J. Mol. Biol.* **1990**, *214*, 585.
35. Lambeth, J. D. Cytochrome P-450scc. Cardiolipin as an effector of activity of a mitochondrial cytochrome P-450. *J. Biol. Chem.* **1981**, *256*, 4757.
36. McClelland, L. J.; Mou, T.-C.; Jeakins-Cooley, M. E.; Sprang, S. R.; Bowler, B. E. Structure of a mitochondrial cytochrome c conformer competent for peroxidase activity. *Proc. Natl. Acad. Sci. U.S.A.* **2014**, *111*, 6648.
37. San Francisco, B.; Bretsnyder, E. C.; Kranz, R. G. Human mitochondrial holocytochrome c synthase's heme binding,

maturation determinants, and complex formation with cytochrome c. *Proc. Natl. Acad. Sci. U.S.A.* **2013**, *110*, E788.
38. Sato, W.; Hitaoka, S.; Inoue, K.; Imai, M.; Saio, T.; Uchida, T.; Shinzawa-Itoh, K.; Yoshikawa, S.; Yoshizawa, K.; Ishimori, K. Energetic Mechanism of Cytochrome C-Cytochrome c Oxidase Electron Transfer Complex Formation under Turnover Conditions Revealed by Mutational Effects and Docking Simulation. *J. Biol. Chem* **2016**, *291* (29), 15320–15331.
39. Nataša, T.; Rastislav, V.; Veronika, L.; Andrej, M.; Erik, S. Peroxidase activity of cytochrome c in its compact state depends on dynamics of the heme region. *Biochim. Biophys. Acta - Proteins Proteom.* **2018**, *1866*, 1073.
40. Krieger, M.; Kay, L. M.; Stroud, R. M. Structure and specific binding of trypsin: comparison of inhibited derivatives and a model for substrate binding. *J. Mol. Biol.* **1974**, *83*, 209.
41. Smith, L.; Davies, H. C.; Nava, M. E. Effect of adenosine 5'-triphosphate and adenosine 5'-diphosphate on the oxidation of cytochrome c by cytochrome c oxidase. *Biochemistry.* **1980**, *19*, 1613.
42. Craig, D. B.; Wallace, C. J. A. ATP binding to cytochrome c diminishes electron flow in the mitochondrial respiratory pathway. *Protein Sci.* **1993**, *2*, 966.
43. Ahn, S.-H.; Seitz, C.; Cruzeiro, V. W. D.; McCammon, J. A.; Götz, A. W. Data for molecular dynamics simulations of Escherichia coli cytochrome bd oxidase with the Amber force field. *Data Br.* **2021**, *38*, 107401.
44. DA, C.; Ben-Shalom, S.; Brozell, D.; Cerutti III, T.; Cheatham III, V.; Cruzeiro, T.; Darden, R.; Duke, D. G.; Gilson, M.; Gohlke, H. AMBER 18. *UCSF.* **2018**.
45. Meagher, K. L.; Redman, L. T.; Carlson, H. A. Development of polyphosphate parameters for use with the AMBER force field. *J. Comput. Chem.* **2003**, *24*, 1016.
46. Junmei, W.; Wei, W.; Peter, A. K.; David, A. C. Automatic atom type and bond type perception in molecular mechanical calculations. *J. Mol. Graph. Model.* **2006**, *25*, 247.
47. He, X.; Man, V. H.; Yang, W.; Lee, T.-S.; Wang, J. A fast and high-quality charge model for the next generation general AMBER force field. *J. Chem. Phys.* **2020**, *153*, 114502.
48. Tian, C.; Kasavajhala, K.; Belfon, K. A. A.; Raguette, L.; Huang, H.; Migues, A. N.; Bickel, J.; Wang, Y.; Pincay, J.; Wu, Q.; Simmerling, C. ff19SB: Amino-acid-specific protein backbone parameters trained against quantum mechanics energy surfaces in solution. *J. Chem. Theory Comput.* **2020**, *16*, 528.
49. Anandakrishnan, R.; Aguilar, B.; Onufriev, A. V. H++ 3.0: automating p K prediction and the preparation of biomolecular structures for atomistic molecular modeling and simulations. *Nucleic Acids Res.* **2012**, *40*, W537.
50. Götz, A. W.; Williamson, M. J.; Xu, D.; Poole, D.; Le Grand, S.; Walker, R. C. Routine microsecond molecular dynamics simulations with AMBER on GPUs. 1. Generalized born. *J. Chem. Theory Comput.* **2012**, *8*, 1542.
51. Zwanzig, R. Nonlinear generalized Langevin equations. *J. Stat. Phys.* **1973**, *9*, 215.
52. Hopkins, C. W.; Le Grand, S.; Walker, R. C.; Roitberg, A. E. Long-time-step molecular dynamics through hydrogen mass repartitioning. *J. Chem. Theory Comput.* **2015**, *11*, 1864.
53. Berendsen, H. J. C.; Postma, J. P. M.; Gunsteren, W. F. v.; DiNola, A.; Haak, J. R. Molecular dynamics with coupling to an external bath. *J. Chem. Phys.* **1984**, *81*, 3684.
54. Doerr, S.; Harvey, M. J.; Noé, F.; De Fabritiis, G. HTMD: high-throughput molecular dynamics for molecular discovery. *J. Chem. Theory Comput.* **2016**, *12*, 1845.
55. Roe, D. R.; Cheatham, III, T. E. PTRAJ and CPPTRAJ : Software for Processing and Analysis of Molecular Dynamics Trajectory Data. *J. Chem. Theory Comput.* **2013**, *9* , 3084.
56. Scherer, M. K.; Trendelkamp-Schroer, B.; Paul, F.; Pérez-Hernández, G.; Hoffmann, M.; Plattner, N.; Wehmeyer, C.; Prinz, J.-H.; Noé, F. PyEMMA 2: A software package for estimation, validation, and analysis of Markov models. *J. Chem. Theory Comput.* **2015**, *11*, 5525.